Structural requirements of *endo*polygalacturonase for the interaction with PGIP (polygalacturonase-inhibiting protein)

L. Federici*†, C. Caprari†‡, B. Mattei†‡, C. Savino*, A. Di Matteo*, G. De Lorenzo‡, F. Cervone‡§, and D. Tsernoglou*

*Dipartimento di Scienze Biochimiche and ‡Dipartimento di Biologia Vegetale, Università di Roma "La Sapienza", Piazzale le Aldo Moro 5, 00185 Rome, Italy

Communicated by Brian J. Staskawicz, University of California, Berkeley, CA, September 6, 2001 (received for review July 19, 2001)

To invade a plant tissue, phytopathogenic fungi produce several cell wall-degrading enzymes; among them, *endo*polygalacturonase (PG) catalyzes the fragmentation and solubilization of homogalacturonan. Polygalacturonase-inhibiting proteins (PGIPs), found in the cell wall of many plants, counteract fungal PGs by forming specific complexes with them. We report the crystal structure at 1.73 Å resolution of PG from the phytopathogenic fungus *Fusarium moniliforme* (*Fm*PG). The structure of *Fm*PG was useful to study the mode of interaction of the enzyme with PGIP-2 from *Phaseolus vulgaris.* Several amino acids of *Fm*PG were mutated, and their contribution to the formation of the complex with PGIP-2 was investigated by surface plasmon resonance. The residues Lys-269 and Arg-267, located inside the active site cleft, and His-188, at the edge of the active site cleft, are critical for the formation of the complex, which is consistent with the observed competitive inhibition of the enzyme played by PGIP-2. The replacement of His-188 with a proline or the insertion of a tryptophan after position 270, variations that both occur in plant PGs, interferes with the formation of the complex. We suggest that these variations are important structural requirements of plant PGs to prevent PGIP binding.

*Endo*polygalacturonases (PGs), produced by a large variety of organisms such as bacteria, fungi, and plants, are involved in many physiological and pathological processes characterized by degradation and remodeling of the plant cell wall. Phytopathogenic microorganisms utilize PG as a component of their offensive arsenal to penetrate and colonize the plant tissues (1). Plants, instead, utilize PG in processes such as growth (2), fruit softening (3), root formation (4), organ abscission (5), and pollen development (6). The complex role of PG in the dynamics of the plant cell wall is suggested by the presence of large PG gene families in plant genomes; e.g., more than 50 putative PGs have been identified in the small plant *Arabidopsis thaliana* (7). Fungal PGs with an *endo* mode of action catalyze the fragmentation and solubilization of pectic polymers by cleaving the internal bonds of homogalacturonan, which is the constituent of the "smooth region" of pectin. The complete hydrolysis of homogalacturonan by fungal PGs can be hampered by polygalacturonase-inhibiting proteins (PGIPs), localized in the cell wall of many plants. PGIPs inhibit and modulate the activity of fungal PGs and favor the release of elicitor-active oligogalacturonides (1). On the other hand, the plant-derived PGs characterized so far do not appear capable of interacting with PGIPs. For example, a tomato fruit PG, involved in fruit softening, is not inhibited by PGIPs (8), which is consistent with the finding that transgenic plants overexpressing PGIPs exhibit a normal fruit softening (9, 10).

PGIPs belong to the large family of the leucine-rich repeat (LRR) proteins (11). In plants, LRR proteins play relevant roles both in resistance and development: the products of several resistance (*R*) genes (12), several orphan receptor kinases of *Arabidopsis* (13–16) and of apple (17) display LRR domains homologous to those of PGIP. We are studying at the molecular level the interaction between PGIPs and fungal PGs as a model to understand LRR-mediated recognition events occurring in plants. Recently, we demonstrated that the residues in the β-strand/β-turn motif of PGIP are critical for its affinity and specificity for the PG ligands (18). Similarly, residues in the β-strand/β-turn motif of some *R* gene products and LRR receptors may also be crucial for ligand binding and recognition specificity. Our studies not only contribute to the comprehension of many important physiological and pathological processes that in plants involve LRR proteins, but also provide the knowledge for the design of improved inhibitors for biotechnological purposes.

In this work, we have investigated the PG–PGIP interaction by looking at the structural requirements of PGs for recognition by PGIPs. Here, we report the structure of PG from the phytopathogenic fungus *Fusarium moniliforme* (*Fm*PG) determined to a resolution of 1.73 Å by x-ray crystallography. By site-directed mutagenesis and surface plasmon resonance (SPR) analysis, we have identified several residues of *Fm*PG critical for the interaction with PGIP-2 from *Phaseolus vulgaris* and addressed the question of how PGs of plant origin may escape the recognition by PGIP and maintain functionality in the presence of PGIP. We report that the modification of the *Fm*PG with residues that are typically found in plant PGs renders the enzyme unable to interact with PGIP.

Materials and Methods

Strains and Media. Strains and media were as already described (19).

Plasmid Construction and Site-Directed Mutagenesis. The pCC6 plasmid DNA previously described (19) was used to transform *Saccharomyces cerevisiae* strain S150-2B. Mutations were introduced into pCC6 plasmid by using the U.S.E. Mutagenesis Kit (Amersham Pharmacia Biotech) according to the manufacturer's instructions. Mutagenic primers were the following oligonucleotides (the mutated codon is underlined): D191A (5′-GCGCATAACACCGCTGGTTTCGACATC-3′), D212E-D213E (5′-CATGTTTATAACCAAGAAGAATGTGTTG-CTGTTACT-3′), D212N-D213N (5′-CATGTTTATAAC-CAAAATAATTGTGTTGCTGTT-3′), K269E (5′-CAGAAT-GGATGTCGCATCGAGTCCAACTCTGGCGCAACT-3′), S270insW (5′-GGATGTCGCATCAAGTCCTGGAACTCTG-GCGCAACTGGC-3′), R267A (5′-CAGAATGGATGTGC-CATCAAGTCCAAC-3′), and H188P (5′-TTGCCCGCT-GCGCCTAACACCGACGGT-3′).

Abbreviations: PG, *endo*polygalacturonase; LRR, leucine-rich repeat; *Fm*PG, *Fusarium moniliforme endo*polygalacturonase; *An*PGII, *Aspergillus niger endo*polygalacturonase II; PGIP, polygalacturonase-inhibiting protein; PGIP-2, *Phaseolus vulgaris* polygalacturonase-inhibiting protein isoform 2.

Data deposition: Coordinates and structure factors for *Fm*PG have been deposited in the Protein Data Bank, www.rcsb.org (PDB ID codes are 1hg8 and r1hg8sf, respectively).

†L.F., C.C., and B.M. contributed equally to this work.

§To whom reprint requests should be addressed. E-mail: felice.cervone@uniroma1.it.

The publication costs of this article were defrayed in part by page charge payment. This article must therefore be hereby marked "*advertisement*" in accordance with 18 U.S.C. §1734 solely to indicate this fact.

PLANT BIOLOGY

Purification and Characterization of PGs. *Fm*PG and mutant *Fm*PGs expressed in yeast were prepared and purified as previously described (19). Protein concentration was determined by the method of Bradford (20).

Enzyme Assays. *Fm*PG activity was determined by reducing end-group analysis as already described (19). One activity unit (RGU, reducing groups unit) was defined as the amount of the enzyme producing 1 μmol of reducing groups per min at 30°C with 0.5% (wt/vol) polygalacturonic acid as substrate.

PGIP Purification. PGIP-2 was purified from PVX-infected tissues of *Nicotiana benthamiana* as previously described (21).

Surface Plasmon Resonance. Measurements were performed as already described (9). Sensorgrams were analyzed with BIAEVALUATION 2.1 software from BIACORE (Uppsala). A single-site binding model (A + B = AB) was used for the analysis. The equilibrium dissociation constant of the interaction, K_D, was determined by a Scatchard analysis from the dependence of the plateau signal at steady state on the concentration of *Fm*PG in the mobile phase.

Crystallography. Single crystals of *Fm*PG were obtained and cryoprotected as already described (22). All data were collected at 100 K. Native data were collected at the ELETTRA Synchrotron beamline (Trieste, Italy), equipped with a Mar345 image plate detector. Best crystals diffracted up to 1.73 Å resolution. Two heavy atom derivatives data sets were also collected. The $Hg(OAc)_2$ data set was collected at ELETTRA, whereas the $Pb(OAc)_2$ data set was collected in house with an R-AXIS II image plate detector mounted on a Rigaku (Tokyo) rotating anode x-ray generator, equipped with a mirror monochromator. All data were processed with DENZO (23) and scaled with SCALA in the CCP4 package (24). *Fm*PG structure was solved by MIRAS (multiple isomorphous replacement and anomalous scattering) methods. Heavy atom positions were searched by using the program SHELXS (25). Two distinguishable and consistent peaks were found for the $Hg(OAc)_2$ derivative. These two heavy metal positions were refined separately by using the program MLPHARE (26), and the best one was selected. By using phases deriving from this first solution, difference Fourier maps were calculated and examined for both derivatives. This process allowed us to identify three distinct heavy atom positions in the $Hg(OAc)_2$ and one in the $Pb(OAc)_2$ derivatives. These positions were refined together with MLPHARE to produce a first set of phases. A density modification procedure based on solvent flattening and histogram matching algorithms was then applied by using the program DM (27). The resulting phases were used as input for the ARP-WARP automated building procedure (28). Phases were first extended to 1.73 Å resolution by warp routine and then the warpNtrace routine was applied. Three hundred twenty-nine amino acid residues of 349 were automatically built into five chains. At this stage, first electron density maps were inspected, and all of the lacking residues and correct side chains were manually built by using the program QUANTA (Molecular Structure, The Woodlands, TX).

Refinement was carried out by using a combined procedure of refining with REFMAC (29) and solvent addition with ARP (30). Water molecules were finally kept in the model only if they had suitable stereochemistry and a *B* factor after refinement below 60 Å^2. Finally, electron density maps were carefully inspected in those regions corresponding to the four putative glycosylation sites of the protein.

The final model consists of 349 amino acid, 3 GlcNAc, and 329 water residues. The geometrical quality of the model was monitored by using program PROCHECK (31). Structure superpositions and rms deviations between Cα with related proteins were performed and calculated by using the program INSIGHT (Molecular Structure).

Modeling. A tryptophan residue, namely S270insW, was inserted in the model structure of *Fm*PG by using the X-AUTOFIT/X-BUILD module of the program QUANTA (Molecular Structure). The side chain orientation was chosen among the most represented rotamers in the program database, manually adjusted in the position where minor clashes with nearby atoms could be observed and checked out for proper geometry by the REGULARIZE utility. The model obtained was subjected to energy minimization by using unrestrained conjugate gradient optimization (Powell algorithm, 500 cycles) as implemented in the program X-PLOR (32).

Results

The Structure of PG from *F. moniliforme*. The sequence of the mature *Fm*PG after the processing of the signal peptide (residues 1–24) includes 349 aa (residues 25–373). The crystal structure of *Fm*PG was solved by multiple isomorphous replacement and anomalous scattering (MIRAS) methods. Details about data collections, phasing, and refinement statistics are summarized in Table 1. The overall architecture consists of a right-handed parallel β-helix (33), resulting from the tandem repetition of 10 coils, each formed by three or four β-strands (Fig. 1*a*). The secondary structure organization of *Fm*PG is summarized in Table 2. The β-strands of consecutive turns line up to form parallel β-sheets indicated as PB1, PB2a, PB2b, and PB3 (names of β-sheets are as those adopted for the pectate lyase C structure; ref. 33). The β-sheet PB2a, starting from the sixth turn of the β-helix, is typical of PGs and is absent in other proteins sharing the same overall fold (34). The length of the β-strands is generally short (3 to 5 residues); more variable is the length of the turns (T) between β-strands. The turns T1 (between PB1 and PB2b or PB2a) and T2 (between PB2b and PB3), and the PG-specific turns between PB2a and PB2b, are very short and often composed by only one residue in α_L conformation; this residue is often an asparagine, which may contribute, through its H-bonding capability, to the significant change in the polypeptide backbone direction. The T3 turns (between PB3 and PB1) are more variable, and their length varies from 3 to 24 residues; these loops determine the formation of a deep cleft on one side of the β-helix (Fig. 1 *a* and *b*), where the putative active site is located. The interior of the β-helix is entirely occupied by apolar side chains, with the exception of the residues in α_L conformation. The β-helix openings are capped on the N-terminal and C-terminal sides by an α-helix and a flexible loop, respectively. Two aromatic stacks are located inside the β-helix, the first formed by residues Phe-254, Tyr-283, Phe-322, and Phe-350, and the second formed by Phe-154 and Phe-193. Aliphatic stacks are also well represented. The architecture of the protein is stabilized by the presence of four disulfide bridges distributed along the β-helix. One is located at the N-terminal end between Cys-27 and Cys-42; two, located approximately in the middle of the β-helix, are formed by Cys-214 and Cys-230, and Cys-340 and Cys-345, respectively; the fourth one is formed by Cys-364 and Cys-371 and determines the C-terminal capping of the β-helix. Four putative N-glycosylation sites are present, at positions 65, 94, 280, and 292; however, an additional electron density is found only corresponding to the first two sites. This density was interpreted by adding one *N*-acetylglucosamine molecule N-linked to Asn-65 and two *N*-acetylglucosamine molecules linked to Asn-94.

*Fm*PG and PGII from *Aspergillus niger* (*An*PGII) have a sequence identity of 43.5%, and their structures are almost completely superimposable, with an average rms deviation between equivalent C_α of 0.97 Å. All secondary structure elements are conserved among the two proteins both in the β-helical region and in the region outside the β-helix. Thirteen of the 15 additional residues of *Fm*PG form two loops that are absent in *An*PGII. The first loop is located inside the T3 turn of the second β-helical turn (residues 120 to 123). The second one is located within the T3 turn of the fifth β-helical turn (residues 177 to 185; Fig. 2).

Table 1. Data collection, phasing, and refinement parameters

Crystal information			
Space group			$P2_12_12_1$
Unit cell dimensions, Å			$a = 58.26$, $b = 61.59$, $c = 98.86$
Molecules per asymm. unit			1
Data collection			
Crystal	Native	$Hg(OAc)_2$	$Pb(OAc)_2$
Soaking time, days		3	1
Metal concentration, mM		5	1
Maximum resolution, Å	1.73	2.5	3.0
Average I/σ	16.6	16.2	12.7
No. of observations	204,193	192,171	15,239
No. of unique reflections	37,710	13,074	6,691
Completeness, %*	99.37 (96.6)	99.9 (99.4)	90.5 (87.9)
R_{merge}*	0.059 (0.302)	0.098 (0.174)	0.087 (0.155)
MIRAS analysis			
Number of positions		3	1
R_{cullis}		0.58	0.97
Isomorphous phasing power		1.57	0.23
Anomalous phasing power		2.00	0.31
Structure refinement			
Resolution, Å			17.9–1.73
No. of unique reflections			37,710
R_{cryst}			0.1728
R_{free}			0.2030
rmsd bond length, Å			0.009
rmsd bond angles, °			2.195
Ramachandran statistics			
% of residues in allowed regions			99.3
% of residue in generously allowed			0.7
% of residue in not allowed			0.0
Model	349 amino acid residues 3 GlcNAc 329 water residues		

*Numbers in parentheses refer to the last resolution shell.

The Residues of PG Interacting with PGIP. Because PGIPs are specific inhibitors of fungal PGs, we were interested in pinpointing the residues involved in the interaction with PGIP. We have targeted several residues of *Fm*PG that are conserved in all of the known fungal PGs. Among them, Asp-191, Asp-212, Asp-213, Arg-267, and Lys-269 are located, as in *An*PGII, inside the deep cleft (35) and form the putative active site (Fig. 1, Fig. 3).

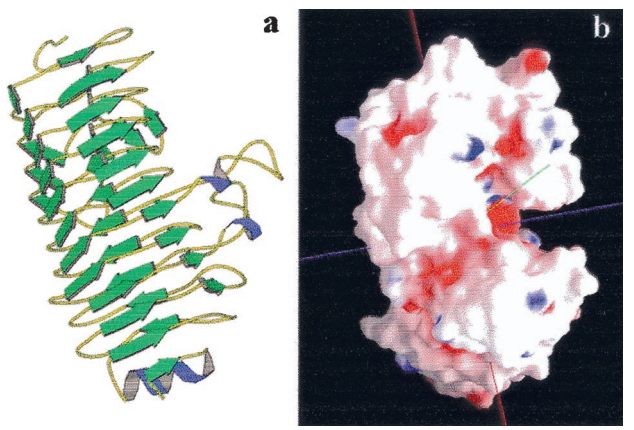

Fig. 1. Structure of *Fm*PG. (*a*) MOLSCRIPT representation of the right-handed parallel β-helix, consisting of 10 coils each made up of three or four β–strands. (*b*) Electrostatic potential surface representation. The model is oriented to highlight the putative active site. Negative charges are shown in red, positive charges in blue.

A water molecule is localized at H-bond distance from Asp-191 (2.59 Å) and Asp-213 (2.75 Å). The single or double mutations Asp191Ala, Asp212Glu-Asp213Glu, Asp212Asn-Asp213Asn, Arg267Ala, and Lys269Glu all drastically affected the enzyme activity (Table 3), indicating that the targeted residues take part in the enzymatic reaction mechanism and/or binding to the substrate. Asp-191, Asp-212, and Asp-213, whose oxygens are all located within 5.4 Å from each other, were modified either non-conservatively or conservatively. Complete enzyme inactivation occurred in each case (Table 3), showing that not only the charge but also the relative distance between these charged groups must be maintained.

The mutation Arg267Ala also leads to an inactive enzyme, whereas the mutation Lys269Glu reduces the enzyme activity to only 0.026% of wild-type activity (Table 3). In analogy with the function of the homologous residues of *An*PGII (35), Arg-267 and Lys-269 likely play a role in substrate binding. The terminal nitrogen of Lys-269 is located 3.02 Å from and interacts with the oxygen OD1 of Asp-213. The nitrogen NH2 of Arg-267 is located at 3.02 Å from, and interacts with, Asp-213 OD2. Given their position in proximity of the nucleophilic water molecule but at opposite sides, and their relative distance of 4.06 Å, Arg-267 and Lys-269 putatively bind the substrate at subsites +1 and −1, respectively (where +1 and −1 are the residues at the reducing and non-reducing ends, respectively; ref. 35).

The effect of the mutations on the binding kinetics of the PG-PGIP interaction was studied by analyzing the various *Fm*PG-mutated proteins on the *P. vulgaris* PGIP-2 immobilized on a sensor chip; the interaction was measured in real time by recording the changes in resonance units. Binding curves (sen-

PLANT BIOLOGY

Table 2. Secondary structure assignment* for the parallel β-helix of *Fm*PG

T	PB1	PB2a	α_L	PB2b	α_L	PB3
				β_1 27–29		β_3 51–52
1	β_4 58–60			β_5 68–71		β_6 74–77
2	β_7 88–93			β_8 96–99		β_9 104–106
3	β_{10} 128–133			β_{11} 139–142		β_{12} 145–147
4	β_{13} 152–157			β_{14} 160–165		β_{15} 168–170
5	β_{16} 193–196			β_{17} 199–204	Asn-205	β_{18} 206–209
6	β_{19} 215–217	β_{20} 218–221	Asn-222	β_{21} 223–226	Asn-227	β_{22} 228–231
7	β_{23} 236–241	β_{24} 248–250		β_{25} 252–255	Ser-256	β_{26} 257–260
8	β_{27} 264–271	β_{28} 276–279	Asn-280	β_{29} 281–284	Asn-285	β_{30} 286–291
9	β_{31} 294–303	β_{34} 315–323	Lys-234	β_{35} 325–329		β_{36} 334–339
10	β_{37} 345–351			β_{38} 354–356		β_{39} 363–364

*The elements of secondary structure were assigned using program PROCHECK (31). Some elements are outside the β-helix; these are the helices α_1 (35–41), α_2 (109–112), and α_3 (172–175), and the β-strands β_{32} (306–307) and β_{33} (310–311).

sorgrams) are shown in Fig. 4 for wild-type *Fm*PG and the mutated proteins. The equilibrium dissociation constants (K_D) were determined for the binding of each PG-mutated protein to PGIP-2 after analysis of several enzyme concentrations in the range 2 nM to 18 μM (Table 3). The mutations Asp191Ala, Asp212Glu-Asp213Glu, and Asp212Asn-Asp213Asn had little or no effect on the interaction between *Fm*PG and PGIP-2: K_D values were comparable with those obtained by using the wild-type enzyme. The mutation Lys269Glu, on the other hand, affected the interaction of the enzyme with PGIP-2: the K_D value was over 12 times higher than that obtained with the wild-type PG. The mutation Arg267Ala also had a considerable effect, given a K_D value for the interaction with PGIP-2 $\approx$14 times higher than for that of the wild-type PG.

Because Arg-267 and Lys-269 putatively bind the substrate at subsites +1 and −1, their engagement in the formation of the complex with PGIP-2 probably prevents the binding of the substrate to the enzyme. This observation is consistent with our findings that PGIP-2, by interacting with *Fm*PG, inhibits the enzyme activity with a competitive mode of action: a Lineweaver-Burk analysis, measuring the enzyme activity in the presence or in the absence of the inhibitor at different substrate concentrations was performed. Whereas the V_{max} is approximately constant, the K_m values calculated from the slopes of the linear fits in the double reciprocal plot vary from 0.56 mg/ml for the enzyme alone to 1.37 mg/ml and 4.68 mg/ml for the same amount of enzyme in presence of increasing concentrations of inhibitor (0.31 ng/μl and 0.43 ng/μl, respectively).

FmPG Modified with Residues Typical of Plant-Derived PGs Is Not Recognized by PGIP. By comparing the available sequences of PGs from fungi and plants, we noticed that His-188, located at the edge of the putative active site cleft, at a distance of 12.2 Å from Lys-269, is conserved in most known fungal PGs and invariably replaced by a proline in all plant-derived PGs. Our experiments show that the mutation of His-188 into a proline drastically affected the interaction of the enzyme with PGIP-2 as witnessed by a K_D value over 40 times higher than that obtained with the wild-type PG (Table 3).

By comparing sequences we also noticed that, after the position

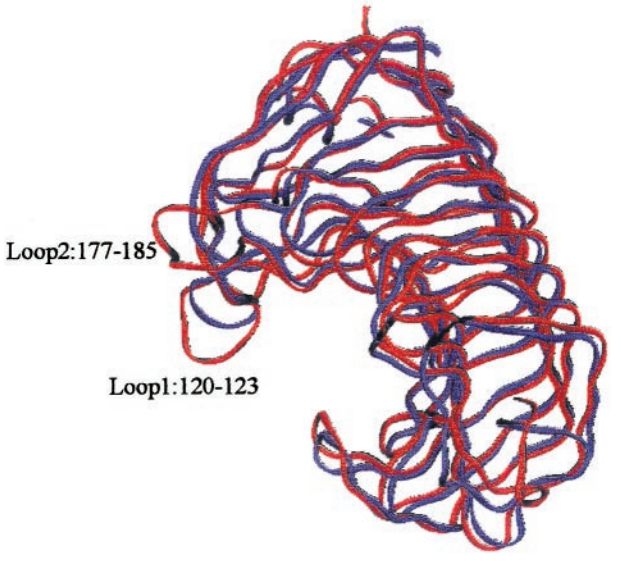

Fig. 2. Structural superposition between *Fm*PG (in red) and *An*PGII (in blue) represented as protein ribbons. The superposition was performed by matching identical residues with the automated procedure implemented in the program INSIGHTII.

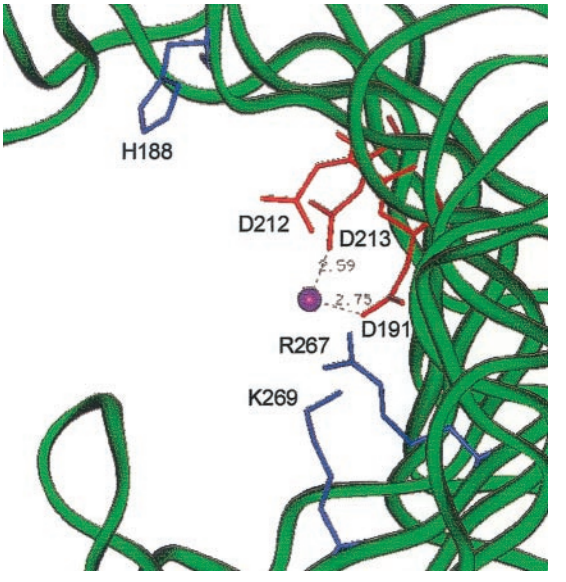

Fig. 3. Overview of the active site of *Fm*PG. According to the proposed mechanism of action (35), three aspartic acids catalyze the reaction; D212 is the general acid, donating a proton to the glycosydic oxygen; D191 and D213 activate a water molecule (shown in magenta) that performs a nucleophilic attack to the anomeric carbon. K269 and R267 are necessary for substrate binding and are involved in binding to PGIP-2 together with H188.

Table 3. Specific activity of mutated PGs and K_D values of their interaction with PGIP-2

	Specific activity, RGU/mg*	K_D, nM
*Fm*PG	500	47.7
D191A	0	93.0
D212E–D213E	0	74.8
D212N–D213N	0	96.4
K269E	0.13	588
R267A	0	665
H188P	1.75	1954
S270insW	1.76	No interaction

*RGU, reducing groups unit.

corresponding to residue 270 of *Fm*PG, plant PGs show a tryptophan residue that is absent in the fungal ones. The insertion of a tryptophan after position 270 in *Fm*PG produced an enzyme (S270insW) with no capacity of interacting with PGIP-2 (Table 3). In both cases, the variant enzymes (H188P and S270insW) resulted to maintain functionality; their specific activities, however, were considerably lower than that of the wild-type enzyme (Table 3), in agreement with the notion that plant-derived PGs are not destructive enzymes and have a much lower activity than microbial PGs. For instance, both banana and tomato PGs were reported to have specific activities 100-fold lower than that of *Fm*PG (ref. 36 and references therein). We hypothesize that the big indolic side chain of the added tryptophan may constitute a considerable steric hindrance inside the active site cleft and form a favorable stacking interaction with the conserved residue Tyr-302, as shown in the model of the S270insW structure superimposed with that of the wild-type enzyme (Fig. 5). At the same time, this insertion may cause a significant movement of the Lys-269 side chain, demonstrated to be important for the interaction with PGIP-2.

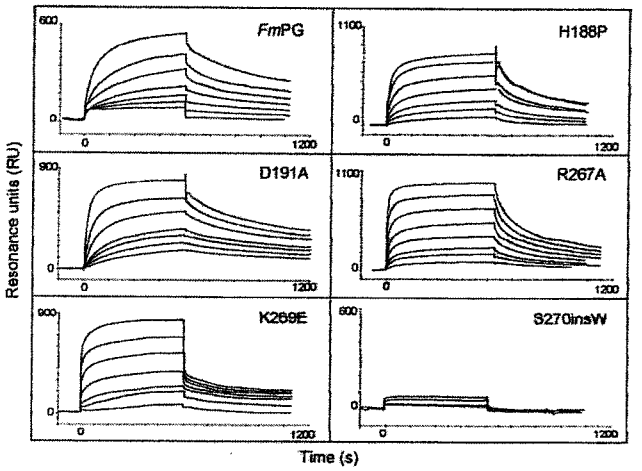

Fig. 4. The interaction between different mutants of *Fm*PG and PGIP-2 from *P. vulgaris* analyzed by using a BIACORE X instrument. The different panels show the surface plasmon resonance (SPR) sensorgrams of the interactions. The *y* axis units are resonance units (RU), which are proportional to the mass of protein binding to PGIP immobilized on the surface of the chip. Each sensorgram can be divided into three phases: association during sample injection, steady state, and dissociation from the surface during buffer flow at the end of the injection. *Fm*PG: Sensorgrams of the interaction between wild-type PG and immobilized PGIP-2. Concentrations of PG used were (from bottom to top curve): 9.5 nM, 12.5 nM, 25 nM, 50 nM, 160 nM, 400 nM, and 800 nM. H188P: Sensorgrams of the interaction between H188P PG and immobilized PGIP-2. Concentrations of PG used were (from bottom to top of curve): 280 nM, 561 nM, 1.12 μM, 2.24 μM, 4.49 μM, 8.98 μM, and 17.96 μM. D191A: Sensorgrams of the interaction between D191A PG and immobilized PGIP-2. Concentrations of PG used were (from bottom to top curve): 50 nM, 80 nM, 124 nM, 210 nM, 420 nM, 840 nM, and 1.68 μM. R267A: Sensorgrams of the interaction between R267A PG and immobilized PGIP-2. Concentrations of PG used were (from bottom to top curve): 80 nM, 160 nM, 320 nM, 0.65 μM, 1.3 μM, 2.6 μM, 5.2 μM, and 10.4 μM. K269E: Sensorgrams of the interaction between K269E PG and immobilized PGIP-2. Concentrations of PG used were (from bottom to top curve): 80 nM, 214 nM, 480 nM, 535 nM, 1.1 μM, 2.1 μM, and 3.2 μM. S270insW: Sensorgrams of the interaction between S270insW PG and immobilized PGIP-2. Concentrations of PG used were (from bottom to top curve): 535 nM, 1.1 μM, 2.1 μM, and 3.2 μM.

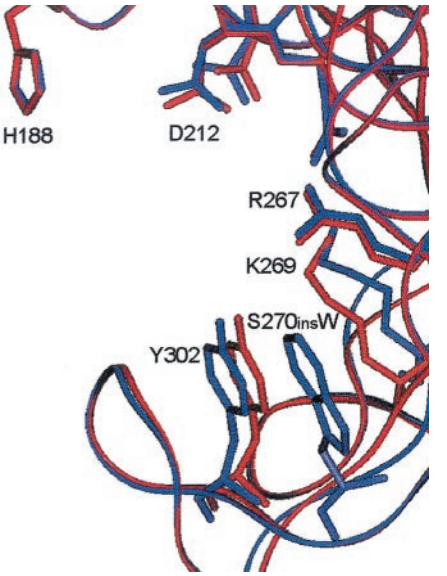

Fig. 5. *Fm*PG structure with the tryptophan residue inserted after position 270 (S270insW). The structure of the wild-type enzyme is shown in red and the model structure of the mutated enzyme in blue.

Discussion

During the last few years the structures of several pectic enzymes have been determined by x-ray crystallography. The determined structures include those of pectin and pectate lyases, which cleave pectin and pectate by a β-elimination mechanism (33, 37), of a rhamnogalacturonase, which acts on the "hairy region" of pectin by hydrolyzing the glycosydic bond between galacturonic acid and rhamnose (38), and of two polygalacturonases, one from the bacterium *Erwinia carotovora* (34) and one from the fungus *A. niger* (*An*PGII) (35). With our determination of the x-ray structure of the PG from *F. moniliforme* (*Fm*PG), we have now complete structural data about two fungal polygalacturonases, the structure of *Fm*PG being the first one from a true phytopathogenic fungus. The sequence identity between *Fm*PG and *An*PGII is 43.5%, and the two proteins maintain a β-helix fold with the same number of turns, the same length and position of β-strands, and the same number and position of disulphide bridges. The two proteins are almost completely superimposable. It remains to establish which features, if any, distinguish a PG of a phytopathogenic fungus from that of a saprophytic fungus.

From the the crystal structure of *Fm*PG we can infer its mode of action. *Fm*PG can be classified into the family 28 of glycosyl hydrolases (39) and, given its structural similarity to the *An*PGII, it is likely to be an inverting enzyme with a non-conventional mechanism of action (35). A single displacement reaction may be catalyzed where an acidic residue acts as a general acid (Asp212) by donating a proton to the glycosydic oxygen, and residues Asp-191 and Asp-213 activate a water molecule, which performs a nucleophilic attack on the anomeric carbon. The unusual distance between the three Asp residues and between Asp-212 and the water molecule is consistent with the suggestion that the proton donation and the nucleophilic attack are performed at the same side with respect

to the α-glycosydic bond to be hydrolyzed (40). It is worth noting the relative low presence of positive charges in the cleft (see Fig. 1*b*). This finding is of some interest in view of the polyanionic nature of the substrate and the fact that bacterial pectate lyases and PGs are generally richer in basic amino acids (34, 41).

It is well known that fungal PGs interact with and are inhibited by plant inhibitors named PGIPs. The interaction between these two kinds of proteins does not explain *per se* why the enzymes are inhibited by the interacting PGIPs. The x-ray structure of *Fm*PG can help us to understand how the enzyme forms a complex with *P. vulgaris* PGIP-2 and why the formation of the complex leads to the inhibition of the enzyme activity. We have established that, like the residues His-234, Ser-237, and Ser-240 reported in a previous paper (19), also the catalytic residues Asp-191, Asp-212, and Asp-213 of *Fm*PG do not form contacts with PGIP-2. Instead, three other residues are important for the formation of the complex: two of them (Lys-269 and Arg-267) are putatively involved in substrate binding whereas to the third one (His-188), located at the opposite side of the active site cleft, has not been ascribed any defined role in catalysis. Therefore, the mechanism of PG inhibition played by PGIPs is possibly dual: the inhibitor prevents interactions necessary for substrate binding and, at the same time, covers the active site cleft. This finding is in agreement with the competitive mode of inhibition that we have experimentally observed for *Fm*PG and PGIP-2. The single mutations in these residues decrease the affinity but do not abolish the interaction completely, indicating that the formation of the complex depends on multiple contacts. In the well-known example of ribonuclease A and its LRR protein inhibitor pRI, a network of interactions is necessary for the formation of the complex (42). His-188, Lys-269, and Arg-267 are conserved at the corresponding positions in *An*PGII and are likely to mediate the interaction of this enzyme with PGIP-2. However, *Fm*PG and *An*PGII not only exhibit different affinities toward PGIP-2, but also different specificities toward other PGIPs: for example, whereas *An*PGII is inhibited by PGIP-1 from *P. vulgaris, Fm*PG is not (18). The two PGs are structurally superimposable (see Fig. 2) except for the presence in *FmPG* of two loops formed by 13 of the 15 additional residues (sequences 120–123 and 177–185). Because of their localization at the edge of the active site cleft, residues in the loop 120–123 are candidates for influencing the interaction with PGIPs.

Because Lys-269 and Arg-267 are putatively involved in substrate binding, they cannot easily mutate without affecting the enzyme activity. Their involvement in the interaction with PGIP therefore minimizes the possibility for a fungal PG to escape recognition. On the other hand, plant PGs are generally not inhibited by PGIPs. In this study, we have addressed the question of how plant PGs may escape recognition and function during growth and development even in the presence of endogenous PGIPs. By comparing the amino acid sequences of fungal and plant PGs, we have noticed that the residue corresponding to His-188 of *Fm*PG, which in the fungal enzymes is located at the entrance of the active site, invariably consists of a proline in plant PGs. Also, in plant PGs a tryptophan residue is inserted after the residue corresponding to the *Fm*PG Ser-270, located at the active site. Notably the adjacent residue Lys-269 is important for the interaction with PGIP-2. We have shown that the replacement of His-188 with a proline determines a decreased affinity of *Fm*PG for PGIP-2, whereas the insertion of a tryptophan inside the active site of *Fm*PG completely abolishes the capability of the enzyme to interact with PGIP-2 possibly through the considerable steric hindrance caused by its side chain. We suggest that both the histidine replacement and the tryptophan insertion in plant PGs respond to the functional need of avoiding the inhibition by endogenous PGIPs.

This paper is in memory of Franco Tatò. We thank Maurizio Brunori for his encouragement and valuable advice. This research was supported by the European Community Grant QLK3-CT99-089, the Institute Pasteur-Fondazione Cenci Bolognetti, the Giovanni Armenise-Harvard Foundation, and the Agenzia Spaziale Italiana (ASI).

1. De Lorenzo, G., D'Ovidio, R. & Cervone, F. (2001) *Annu. Rev. Phytopathol.* **39,** 313–335.
2. Futamura, N., Mori, H., Kouchi, H. & Shinohara, K. (2000) *Plant Cell Physiol* **41,** 16–26.
3. Wang, Z. Y., MacRae, E. A., Wright, M. A., Bolitho, K. M., Ross, G. S. & Atkinson, R. G. (2000) *Plant Mol. Biol.* **42,** 317–328.
4. Peretto, R., Favaron, F., Bettini, V., De Lorenzo, G., Marini, S., Alghisi, P., Cervone, F. & Bonfante, P. (1992) *Planta* **188,** 164–172.
5. Kalaitzis, P., Solomos, T. & Tucker, M. L. (1997) *Plant Physiol.* **113,** 1303–1308.
6. Allen, R. L. & Lonsdale, D. M. (1993) *Plant J.* **3,** 261–271.
7. Torki, M., Mandaron, P., Mache, R. & Falconet, D. (2000) *Gene* **242,** 427–436.
8. Cervone, F., De Lorenzo, G., Pressey, R., Darvill, A. G. & Albersheim, P. (1990) *Phytochemistry* **29,** 447–449.
9. Desiderio, A., Aracri, B., Leckie, F., Mattei, B., Salvi, G., Tigelaar, H., Van Roekel, J. S. C., Baulcombe, D. C., Melchers, L. S., De Lorenzo, G. *et al*. (1997) *Mol. Plant-Microbe Interact.* **10,** 852–860.
10. Powell, A. L., van Kan, J., ten Have, A., Visser, J., Greve, L. C., Bennett, A. B. & Labavitch, J. M. (2000) *Mol. Plant-Microbe Interact.* **13,** 942–950.
11. Mattei, B., Bernalda, M. S., Federici, L., Roepstorff, P., Cervone, F. & Boffi, A. (2001) *Biochemistry* **40,** 569–576.
12. Hammond-Kosack, K. E. & Jones, J. D. G. (1997) *Annu. Rev. Plant Physiol. Plant Mol. Biol.* **48,** 575–607.
13. Torii, K. U., Mitsukawa, N., Oosumi, T., Matsuura, Y., Yokoyama, R., Whittier, R. F. & Komeda, Y. (1996) *Plant Cell* **8,** 735–746.
14. Clark, S. E., Williams, R. W. & Meyerowitz, E. M. (1997) *Cell* **89,** 575–585.
15. Jinn, T. L., Stone, J. M. & Walker, J. C. (2000) *Genes Dev.* **14,** 108–117.
16. Li, J. & Chory, J. (1997) *Cell* **90,** 929–938.
17. Komjanc, M., Festi, S., Rizzotti, L., Cattivelli, L., Cervone, F. & De Lorenzo, G. (1999) *Plant Mol. Biol.* **40,** 945–957.
18. Leckie, F., Mattei, B., Capodicasa, C., Hemmings, A., Nuss, L., Aracri, B., De Lorenzo, G. & Cervone, F. (1999) *EMBO J.* **18,** 2352–2363.
19. Caprari, C., Mattei, B., Basile, M. L., Salvi, G., Crescenzi, V., De Lorenzo, G. & Cervone, F. (1996) *Mol. Plant-Microbe Interact.* **9,** 617–624.
20. Bradford, M. M. (1976) *Anal. Biochem.* **72,** 248–254.
21. Cervone, F., De Lorenzo, G., Degrà, L., Salvi, G. & Bergami, M. (1987) *Plant Physiol.* **85,** 631–637.
22. Federici, L., Mattei, B., Caprari, C., Savino, C., Cervone, F. & Tsernoglou, D. (1999) *Acta Crystallogr. D. Biol. Crystallogr.* **55,** 1359–1361.
23. Otwinoski, Z. & Minor, W. (1996) *Methods Enzymol*. **276,** 307–326.
24. Collaborative Computational Project No.4 (1994) *Acta Crystallogr. D. Biol. Crystallogr.* **50,** 760–767.
25. Sheldrick, G. M., Dauter, Z., Wilson, K. S., Hope, H. & Sieker, C. (1993) *Acta Crystallogr. D. Biol. Crystallogr.* **49,** 18–23.
26. Otwinoski, Z. (1991) in *Isomorphous Replacement and Anomalous Scattering*, eds. Wolf, W., Evans, P. R. & Leslie, A. G. W. (Science and Engineering Research Council, Warrington, U.K.), pp. 80–86.
27. Cowtan, K. (1994) *Joint CCP4 ESF-EACBM Newsletter on Protein Crystallogr.* **31,** 34–38.
28. Perrakis, A., Morris, R. & Lamzin, V. S. (1999) *Nat. Struct. Biol.* **6,** 458–463.
29. Murshudov, G. N., Vagin, A. A. & Dodson, E. J. (1997) *Acta Crystallogr. D. Biol. Crystallogr.* **53,** 240–255.
30. Lamzin, V. S. & Wilson, K. S. (1993) *Acta Crystallogr. D. Biol. Crystallogr.* **49,** 129–147.
31. Laskowski, R. A., Moss, D. S. & Thornton, J. M. (1993) *J. Mol. Biol.* **231,** 1049–1067.
32. Brunger, A. T., Kuriyan, J. & Karplus, M. (1987) *Science* **235,** 458–460.
33. Yoder, M. D., Keen, N. T. & Jurnak, F. (1993) *Science* **260,** 1503–1507.
34. Pickersgill, R., Smith, D., Worboys, K. & Jenkins, J. (1998) *J. Biol. Chem.* **273,** 24660–24664.
35. van Santen, Y., Benen, J. A., Schroter, K. H., Kalk, K. H., Armand, S., Visser, J. & Dijkstra, B. W. (1999) *J. Biol. Chem.* **274,** 30474–30480.
36. Pathak, N. & Sanwal, G. G. (1998) *Phytochemistry* **48,** 249–255.
37. Mayans, O., Scott, M., Connerton, I., Gravesen, T., Benen, J., Visser, J., Pickersgill, R. & Jenkins, J. (1997) *Structure* **5,** 677–689.
38. Petersen, T. N., Kauppinen, S. & Larsen, S. (1997) *Structure* **5,** 533–544.
39. Henrissat, B. (1991) *Biochem. J.* **280,** 309–316.
40. Armand, S., Wagemaker, M. J., Sanchez-Torres, P., Kester, H. C., van Santen, Y., Dijkstra, B. W., Visser, J. & Benen, J. A. (2000) *J. Biol. Chem.* **275,** 691–696.
41. Scavetta, R. D., Herron, S. R., Hotchkiss, A. T., Kita, N., Keen, N. T., Benen, J. A. E., Kester, H. C. M., Visser, J. & Jurnak, F. (1999) *Plant Cell* **11,** 1081–1092.
42. Kobe, B. & Deisenhofer, J. (1995) *Nature (London)* **374,** 183–186.